



34 promoted osteogenic differentiation and angiogenesis in vitro. Finally, we  
35 established GC-ONFH rat model, then, a certain amount of transfected or  
36 controlled BMSCs were injected into the tibia of the rats. Immunohistological  
37 staining and micro-CT scanning results showed that the transplanted  
38 experiment group had significantly promoted more bone regeneration, vessel  
39 volume and the expressions of Runx2, ALP, COL I , VEGF and CD31 when  
40 compared with the effects of the negative or control groups. This study  
41 demonstrated for the first time that the Cx43 overexpression in BMSCs could  
42 promote bone regeneration as seen in the osteogenesis and angiogenesis  
43 process, suggesting that Cx43 may serve as a therapeutic gene target for  
44 GIONFH treatment.

45

46 **Keywords:** Connexin43; glucocorticoids; osteonecrosis of the femoral head;  
47 osteogenesis; angiogenesis

48

## 49 **Background**

50 Glucocorticoids are important therapeutic agents that have been widely used  
51 as anti-inflammatory and immunosuppressive drugs(6, 33, 45, 47). However,  
52 their therapeutic benefits are often associated with serious complications, such  
53 as osteocyte apoptosis and osteonecrosis(8, 15, 43). Osteonecrosis of the  
54 femoral head (ONFH) is a destructive disease that is characterized by cell  
55 death within the femoral head, progressive degeneration of the hip joint, and  
56 severely lowered quality of life(27, 55). Identified risk factors for ONFH include  
57 glucocorticoids use, alcohol consumption and trauma, but its pathogenesis  
58 remains poorly understood. Surgical intervention is currently a traditional  
59 treatment strategy for ONFH; however, it is an invasive procedure and could  
60 influence the patients' quality of life. Therefore, investigating non-surgical  
61 treatment methods for ONFH is necessary.

62 Bone marrow-derived stromal stem cells (BMSCs) have the potential for  
63 self-renewal and multi-directional differentiation and have been widely used in

64 tissue regeneration or repair(4-5, 9, 51, 59). BMSCs are suitable for clinical  
65 applications and are easily obtained from patients, and immunological  
66 incompatibilities could be avoided with autologous transplantation(18, 30).  
67 Preclinical studies showed that bone healing began two weeks after  
68 autologous bone marrow stem cell transplantation for ONFH treatment and  
69 achieved complete healing after nine weeks(42). A follow-up study of five years  
70 showed that the clinical effects of autologous bone marrow cells  
71 transplantation combined with autogenous iliac cancellous bone grafts for the  
72 treatment of moderate lesion of ONFH are comparable to femoral  
73 head-preserving surgeries, suggesting that BMSCs transplantation is a  
74 promising method for ONFH treatment(24). Numerous studies in the literature  
75 had demonstrated the effectiveness of stem cell transplantation in the  
76 treatment of early stages of osteonecrosis(12, 19-20, 57). Hernigou P et al.  
77 found that autologous bone marrow transplantation significantly improved the  
78 natural course of the early stage of ONFH when compared with simple nucleus  
79 pulposus decompression surgery(19). Furthermore, it was found that  
80 P-glycoprotein (P-gp)-overexpression BMSC transplantation could decrease  
81 the risk of glucocorticoids-induced ONFH (GIONFH)(16), and SDF-1 $\alpha$   
82 overexpression of BMSCs could promote osteogenesis and vascularization,  
83 therefore reduce the incidence of GIONFH(54); In addition, the elevated  
84 expression of BMP-2 and BFGF in BMSCs could accelerate bone repair of  
85 ONFH(39). All these findings indicate that there are a variety of factors that  
86 play important roles in the therapeutic effects of BMSCs on ONFH, and we  
87 believe that transplantation of genetically modified BMSCs can be used as an  
88 effective method for the treatment of earlystage GIONFH. Nevertheless, the  
89 pathogenesis of GIONFH is not fully understood, and it's important to further  
90 study the precise mechanisms of GIONFH and find new methods to inhibit or  
91 delay osteonecrosis occurrence.

92 Gap junction channels are formed by two hemichannels, which are  
93 composed of six transmembrane proteins called connexins(23, 25). It has been

94 reported that these connexins play a vital role in tissue homeostasis(7), in the  
95 regulation of cell proliferation and growth, and in cell differentiation and  
96 development(1, 40). There are at least 21 different human connexins that have  
97 been reported in the literature **so far**, and they have a series of homologs that  
98 showed different tissue or cells specificities(2, 29). Among these connexins,  
99 connexin43 (Cx43) is considered to be the main component of gap junctions in  
100 hematopoietic tissue(29). Moorer & Stains reported that Cx43 is greatly  
101 associated with the process of osteogenesis and osteoblast function(35). Li et  
102 al. also reported that Cx43 had the function of regulating extracellular  
103 signal-regulated kinase (ERK) activity, therefore, it consequently regulates  
104 Runx2, which is an essential transcription factor for osteoblast  
105 differentiation(31). In addition, several studies have demonstrated that Cx43 is  
106 greatly involved in the process of angiogenesis(49), which is essential for  
107 osteogenesis. More importantly, the knockdown of Cx43 expression in the  
108 endothelial progenitor cells could decrease the expression of VEGF, and  
109 weaken the angiogenic potential of the cells(50). Furthermore, the use of high  
110 doses of dexamethasone could inhibit the osteogenesis and angiogenesis in  
111 bone tissue(53, 56), and could also down-regulate the expression of Cx43(44).  
112 Based on the facts that osteogenesis and angiogenesis are essential for bone  
113 regeneration, we speculated that Cx43 may play a critical role in GIONFH  
114 treatment. This present work aimed to examine the function of Cx43 in  
115 BMSCs-induced osteogenesis and angiogenesis for GIONFH treatment.

116

## 117 **MATERIALS AND METHODS**

118

### 119 **Rat BMSCs isolation and transfection**

120 BMSCs were isolated from SD rats (males, four weeks old, body weight  
121 100±15 g) as previously described(63). A total of 1-2 ml bone marrow was  
122 aspirated by a heparinized syringe from the lateral tibial tubercle of the rats.  
123 The cells were cultured in low-glucose DMEM supplemented with 10% fetal

124 bovine serum (FBS, Gibco, USA) and 1% penicillin–streptomycin in humidified  
125 atmosphere of 5% CO<sub>2</sub> at 37°C. The cells were passaged when they reached  
126 100% confluence, and after three to five passage, the cells were analyzed by  
127 flow cytometry and kept for further use.

128 Third-passage BMSCs were transfected with a lentiviral plasmid carrying the  
129 green fluorescent protein (GFP) and Cx43 (GeneChem, Shanghai, China) or a  
130 lentiviral plasmid carrying GFP and a negative control sequence (GeneChem,  
131 Shanghai, China). The two groups of the transfected cells were called  
132 Cx43-GFP-BMSCs and GFP-BMSCs, whereas the non-transfected cells were  
133 labeled the Control group. After 12 h of transfection, the medium was replaced  
134 with fresh complete medium, and the transfected cells with a density of more  
135 than 80% confluency were purified using complete medium containing 3 µg/ml  
136 puromycin for 5-6 days.

137

### 138 **Flow cytometry**

139 For phenotypic characterization analysis, 5×10<sup>5</sup> BMSCs were incubated with  
140 fluorescein CD34, CD45, CD29, and CD90 at a dilution rate of 1:100 for 30 min  
141 at 4°C, and then flow cytometry analysis was carried out using a flow  
142 cytometer (BD FACSAria, USA). FlowJo 7.6.5 software (Tree Star Inc.,  
143 Ashland, OR, USA) was used for data analysis. The cells that treated by  
144 puromycin were suspended with culture medium and subjected for further use.

145

### 146 **Real-time polymerase chain reaction (RT–PCR)**

147 Total RNA was extracted from the BMSCs, HUVECs and the rats' femoral  
148 heads using the TRIzol (Invitrogen, USA) method according to the  
149 manufacturer's instructions. RNA was reverse-transcribed to cDNA according  
150 to the manufacturer's instructions (Thermo, USA). The expression levels of  
151 Cx43, Runx2, ALP, and COL I at the mRNA level were measured with IQ<sup>TM</sup>  
152 SYBR Green Supermix (Bio–RAD). The following primers were provided by  
153 TsingKe (Beijing, China): Cx43 forward: 5'-CTCACCTTTGTGCCTTCC-3',

154 reverse: 5'-CTCACCTCCCTGATGCTAA-3'; Runx2 forward:  
155 5'TCGGAAAGGGACGAGAG-3'; reverse: 5'-TTCAAACGCATACCTGCAT-3';  
156 ALP forward: 5'-CCGCAGGATGTGAACTACT-3'; reverse:  
157 5'-GGTACTGACGGAAGAAGGG-3'; COL I :  
158 5'-TGCAAGAACAGCGTAGCC-3'; reverse: 5'-CAGCCATCCACAAGCGT-3';  
159 VEGF forward: 5'-ACAGGGAAGACAATGGGA-3'; reverse:  
160 5'-CTGGAAGTGAGCCAACG-3'; CD31 forward:  
161 5'-TCCCCACCCAAAGTAGC-3'; reverse: 5'-TAAACAGCGCCTCCCAT-3'.

162 PCR was performed for 40 cycles, and the expression levels of mRNAs were  
163 calculated by the  $2^{-\Delta\Delta Ct}$  method, and GAPDH was used as a reference gene.  
164 All experiments were repeatedly performed in three times.

165

### 166 **Western blot analysis**

167 Proteins were extracted using ice-cold RIPA buffer (Beyotime Biotechnology,  
168 China) containing 1 mmol/L PMSF. Lysates mixture was then centrifuged at  
169 14000 rpm for 15 min, and the concentration of protein in the supernatant was  
170 measured by a BCA Protein Assay kit (Beyotime Biotechnology, China). The  
171 proteins samples (20  $\mu$ g/lane) were separated by SDS–PAGE and transferred  
172 onto PVDF membranes (0.45 $\mu$ m, Millipore, USA) using a transfer unit  
173 (Bio–RAD, USA). Thereafter, the membranes were blocked in TBS solution  
174 containing 5% non-fat milk for 2 h at room temperature, and then incubated  
175 with primary antibodies including Cx43 (mouse, 1:1000, abcam), Runx2 (rabbit,  
176 1:1000, Boster Bio), ALP (rabbit, 1:500, Boster Bio), COL I (rabbit, 1:1000,  
177 Boster Bio), VEGF (mouse, 1:1000, abcam), CD31 (mouse, 1:1000, abcam)  
178 and GAPDH (mouse, 1:1000, Sigma–Aldrich) for overnight at a temperature of  
179 4°C, respectively. After been washed with TBST, the membranes were  
180 incubated with secondary antibody (1:10000, ZSBIO, Beijing, China) for two  
181 hours. After been washed with TBST three times, the membranes were  
182 visualized by enhanced chemiluminescence (ECL, Beyotime). The digitized  
183 images were analyzed using IPP software 6.0 (Media Cybernetic, USA).

184

### 185 **Immunofluorescence staining**

186 The osteoblasts were cultured on small coverslips, and allowed to adhere, and  
187 then were treated either with or without  $10^{-6}$  mol/L MPS for four days.  
188 Thereafter, the cells in the two groups were washed with PBS solution for 5  
189 min each, then fixed with 4% paraformaldehyde for 30 min, and washed with  
190 PBS for 5 min each. The cells were also permeabilized with 0.3% Triton X-100  
191 for 20 min, and washed in PBS for 5 min. Then the cells were blocked for 30  
192 min with 10% goat serum at 37°C, and the cells of both groups were incubated  
193 with Cx43 (mouse, 1:200; Santa Cruz, CA, USA), Runx2 (rabbit, 1:300; Boster  
194 Bio, China), ALP or COL I (rabbit, 1:1000, Boster Bio) for overnight at 4°C.  
195 The next day, the cells were washed in PBS three times, and the cells of both  
196 groups were incubated with secondary antibodies (FITC-conjugated  
197 anti-mouse, 1:300; AlexaFluor 488-conjugated anti-rabbit, 1:300) for 2 h at  
198 room temperature. Finally, samples of both groups were incubated with DAPI  
199 for 10 min at room temperature. The images were acquired with a  
200 fluorescence microscope (Zeiss, Carl Zeiss, Germany).

201

### 202 **Inducing Osteogenic differentiation**

203 Total of  $2 \times 10^4$  cells/cm<sup>2</sup> were seeded in a 24-well plate precoated with Gelatin  
204 solution and allowed to adhere. The cells were then treated with osteogenic  
205 differentiation induction medium containing Glutamine, Ascorbate,  $\beta$ -sodium  
206 glycerophosphate, and penicillin–streptomycin (Cyagen, Shanghai, China).  
207 The induction medium was being replaced every three days. Alizarin red  
208 staining assay kit was applied used to detect the mineralization of BMSCs.

209

### 210 **Adipogenic differentiation induction**

211 For achieving adipogenesis, the cells were incubated with the  
212 adipogenesis-inducing medium A (Cyagen, Shanghai, China) for three days,  
213 and then this medium was replaced with the adipogenesis-inducing medium B

214 (Cyagen, Shanghai, China), continuing incubation which was incubated for two  
215 days, and then replaced back with medium A for three days. After 14 days, the  
216 cells were harvested and stained with Oil Red O for 30 min.

217

### 218 **Chondrogenic differentiation induction**

219 A total of  $6 \times 10^5$  cells were put into a 15-ml sterile centrifuge tube and  
220 centrifuged at 250 g for 4 min. The suspension was discarded, and a 0.5ml of  
221 chondrogenic differentiation induction medium without TGF- $\beta$ 3 was added to  
222 resuspend the cells. Then, the cells were washed by repeating the process  
223 above. Thereafter, the cells were treated with chondrogenic differentiation  
224 induction medium containing Dexamethasone, Ascorbate, ITS supplement,  
225 Sodium pyruvate, Proline, and TGF- $\beta$ 3 for three weeks according to the  
226 manufacturer's instruction (Cyagen, Shanghai, China). Frozen slices of the  
227 chondrocytes balls were made and measured by Saffron O staining and  
228 observed under a light microscope (Leica, Japan).

229

### 230 **Cell counting kit-8**

231 Cell Counting Kit-8 (CCK-8) assays (Dojindo, Japan) were used to investigate  
232 the cell proliferation. In a brief, the intervened or control cells were trypsinized  
233 and replanted into 96-well plates with  $5 \times 10^3$  cells/well for the proliferation  
234 assay. Then, a 100  $\mu$ l of DMEM containing 10  $\mu$ l of CCK-8 working solution  
235 was added into each well at the 1, 2, and 3 d time points and incubated for  
236 three hours in an incubator. After the incubation, the optical density at 450 nm  
237 of absorbance was detected with a microplate reader.

238

### 239 **Cell apoptosis**

240 After overexpression of Cx43 in BMSCs, the cells were collected and  
241 incubated with Annexin V-FITC/PI apoptosis detection working solution  
242 (Becton Dickinson) according to the instructions (Becton Dickinson). Then,  
243 flow cytometry analysis was carried out using Flow cytometer (BD FACSAria,



244 USA) and the FlowJo 7.6.5 software (Tree Star Inc.) was used for data  
245 analysis.

246

### 247 **ALP staining**

248 All groups of BMSCs were cultured in 24-well plates at a density of  $2 \times 10^4$   
249 cells/well. Ten days after the osteogenic differentiation induction process on  
250 different groups of BMSCs, including the control group, GFP-BMSCs and  
251 Cx43-GFP-BMSCs, the cells were incubated with BCIP/NBT ALP Color  
252 Development Substrate (Beyotime, Shanghai, China) for 20 min. Thereafter,  
253 the cells were lysed in radioimmunoprecipitation assay lysis buffer  
254 (Sigma–Aldrich) to measure the activity of ALP. ALP activity was evaluated  
255 using an ALP assay kit (Nanjing Jiancheng Biotechnology Co., Ltd., Nanjing  
256 China). The optical density was measured with a microplate reader at 520 nm.

257

### 258 **Alizarin red staining**

259 After twenty-one days, the osteogenic differentiation induction mediums of all  
260 groups were discarded, and gently washed twice with PBS solution. Then, they  
261 were fixed with 4% paraformaldehyde for 30 min; staining with alizarin red for  
262 20 min; and finally observed under a light microscope (Olympus, Japan). To  
263 quantify the mineralization, the calcium deposits were desorbed using 10%  
264 cetylpyridinium chloride (Sigma), and the absorbance at 570 nm was  
265 measured.

266

### 267 **Cell migration assay**

268 Cell migration was evaluated by scratch wound assay, which was described in  
269 detail in our previous study(21). Briefly, the HUVECs were planted into a 6-well  
270 plate at a density of  $5 \times 10^5$  cells/well and cultured in growth medium until the  
271 confluence of the cells reached 100%, the cells were then scratched with  
272 sterile 200 $\mu$ l pipet tips, and the cells debris were removed by PBS solution.  
273 Thereafter, the cells were put back into the incubator (37°C, 5% CO<sub>2</sub>) after

274 adding the conditioned medium that containing 2% FBS. The migration of cells  
275 was photographed under a microscope with Zen Imaging software after 24  
276 hours of scratching. The method for calculating the percentage of wound  
277 healing was in consistent with our previous study(60).

278

### 279 **Tube formation assay**

280 To investigate the effect of Cx43-GFP-BMSCs on the angiogenic differentiation  
281 of HUVECs, we collected the culture supernatants from the different treated  
282 groups of BMSCs to be kept as conditioned mediums for further uses.  
283 HUVECs were seeded into 6-well plates ( $1 \times 10^5$  cells per well) and cultured  
284 with BMSCs-conditioned medium for 3 days. Thereafter, the  
285 angiogenic-associated genes, including VEGF and CD31, were detected by  
286 Western blot analysis.

287 To investigate the angiogenic effects of BMSCs-conditioned medium on  
288 HUVECs, the tube formation assay was performed. In a brief, Matrigel  
289 (50 $\mu$ L/well, Corning, USA) was placed into a 96-well plate on ice and kept for  
290 30 min at 37°C until it became solidified. Subsequently,  $2 \times 10^4$  HUVECs/well  
291 were seeded on the surface of Matrigel and incubated with either  
292 BMSCs-conditioned medium or normal culture medium. Twelve hours later,  
293 tube formation was observed with a light microscope (Olympus, Japan). The  
294 ability to form capillary-like structures was determined by the number of branch  
295 points and tubule lengths in three randomly selected fields under the  
296 microscope.

297

### 298 **Animal model and grouping**

299 All animal experiments were performed based on the guidelines that  
300 formulated by the National Institution of Health on the humane use and care of  
301 laboratory animals, and all animal protocols were granted by the Institutes  
302 Animal Care and Use Committee of West China Medical School of Sichuan  
303 University. A total of 24 adult male Sprague–Dawley (SD) rats (450-500g) were

304 purchased from the experimental animal center of Sichuan University. All rats  
305 were housed at the Animal Center of Sichuan University and kept for eight  
306 weeks.

307 The rats were weighted and randomly divided into four groups, including the  
308 normal group (control, non-transplantation), MPS group (GIONFH,  
309 non-transplantation), negative control group (transplantation of GFP-BMSCs),  
310 and experiment group (transplantation of Cx43-GFP-BMSCs). Based on our  
311 previous study(63), we adopted LPS & MPS to establish the ONFH model. Two  
312 weeks after the first MPS injection, amount of BMSCs ( $1 \times 10^7$  GFP-BMSCs or  
313 Cx43-GFP-BMSCs) were injected into the tibia of the rats in the intervened  
314 groups, whereas the rats in the control or MPS groups had not received any  
315 treatment.

316

### 317 **Micro-CT scanning**

318 As described in our previous study, the femoral head morphologic changes  
319 were detected by a micro-computed tomography (micro-CT) system (Inveon  
320 Multimodality Gantry STD CT) at a resolution of 9  $\mu\text{m}$  with the following  
321 parameters: current, 112  $\mu\text{A}$ ; x-ray energy, 80 kVp; and exposure time, 370  
322 milliseconds. To evaluate the bone morphological changes in the femoral head,  
323 the parameters of new bone volume/total volume (BV/TV), trabecular  
324 thickness (Tb. Th), trabecular number (Tb. N), and trabecular separation  
325 (Tb,Sp) were calculated. To evaluate the angiogenesis, 3D reconstructions  
326 images of blood vessels were obtained, and morphometric parameters,  
327 including blood vessel areas and total blood vessel length in the femoral head,  
328 were calculated.

329

### 330 **Angiography**

331 Angiography was performed as previously described(48). In a brief, eight  
332 weeks after the operation, the rats were anesthetized and perfused with  
333 Microfil (Microfil MV-122; Flow Tech, Carver, MA, USA). The method was as

334 followed: firstly, the hair of the chest was shaved, and the rib cage was  
335 opened with a pair of scissors. Then, a 100ml of heparinized saline and 20ml  
336 of Microfil were continuously injected into the cardiac apex at a rate of 2ml/min.  
337 Finally, the perfused rats were laid flat at 4°C in the refrigerator overnight to  
338 ensure complete polymerization. The bilateral femoral heads were dissected  
339 and harvested, and decalcified in 10% EDTA solution for about 4 weeks; and  
340 the samples were scanned by micro-CT as described above, and the blood  
341 vessels in the femoral head were reconstructed using CTVol software.

342

### 343 **Histology and Immunohistochemistry (IHC)**

344 Hematoxylin and eosin (H&E) staining was applied to assess the  
345 histomorphological changes in the femoral head. After the rats were sacrificed,  
346 their femoral heads were harvested, decalcified, and sectioned in the coronal  
347 plane. Some of the sections were subjected to H&E staining to evaluate the  
348 trabecular structures. Briefly, after fixed with 10% formalin for 24 h, the femoral  
349 heads were decalcified in Ethylene diamine tetraacetic acid (EDTA, 10%)  
350 solution for approximate 4 weeks, and then embedded in paraffin. Samples  
351 were cut into 4µm thick sections, deparaffinized in xylene, dehydrated in a  
352 gradient of ethyl alcohol, and washed 3 times with distilled water. H&E staining  
353 was performed to observe the rate of empty osteocytes lacunae and the  
354 destruction degree of bone trabecula. The software of Image-Pro Plus 6.0  
355 (Media Cybernetics, Baltimore, MD, USA) was used to count the rate of the  
356 empty osteocytes lacunae, and the specific methods were described  
357 previously(61).

358 The expressions levels of Runx2, ALP, COL I , VEGF and CD31 were  
359 detected by immunohistochemistry. In a brief, the tissues were embedded with  
360 paraffin and conventionally sliced into 4µm thick sections. The sections were  
361 baked for 2 h at 60°C before dewaxed in xylene, and rehydration through  
362 graded ethanol. Subsequently, they were placed into sodium citrate buffer pH  
363 6.0 and heated up to 100°C for 5 min for antigen repair. After cooling down, the

364 sections were incubated with 5% goat serum (Solarbio, China) at 37°C for 30  
365 min, then the sections were incubated with rabbit anti-rat Runx2 monoclonal  
366 antibodies (rabbit, 1:1000, Boster Bio), ALP (rabbit, 1:1000, Boster Bio), COL  
367 I (rabbit, 1:1000, Boster Bio), VEGF (mouse, 1:1000, abcam), and CD31  
368 (mouse, 1:1000, abcam) at 4°C for overnight, and lastly incubated with the  
369 secondary antibody (1:1000; biotinylated goat anti-mouse IgG, ZSBIO, China)  
370 at 37°C for one hour. The sections were developed with diaminobenzidine  
371 (DAB; Beyotime Biotechnology, China) to detect the targeted antibody. After  
372 staining, the sections were sealed up with balsam before being observed  
373 under an optical microscope (Olympus Optical, China). The brownish-yellow  
374 that showed color in the cytoplasm or cytomembrane indicated positive results,  
375 and other findings indicated negative results. Five fields were randomly  
376 selected for detection to calculate the positive expression. The experiments  
377 were repeatedly performed three times.

378

### 379 **Statistical analysis**

380 All data were analyzed using SPSS 22.0 software (SPSS, IBM Corporation,  
381 USA), and were presented as the mean  $\pm$  SD. Statistical significant differences  
382 between two groups were analyzed with the Student's t-test, and the  
383 significance among multiple groups was analyzed using one-way ANOVA with  
384 Tukey's post hoc multiple comparison tests, respectively. A correlation analysis  
385 was carried out using a two-tailed Spearman's rank correlation coefficient (r). A  
386 P value < 0.05 was regarded as statistically significant. All experiments were  
387 repeated at least three times.

388

### 389 **Results**

390

#### 391 **Characterization of BMSCs and transfection efficiency**

392 The characteristics of the isolated cells were determined by flow cytometry  
393 method. The cells were positive for CD29 and CD90, but negative for CD34

394 and CD45 (Fig. 1A), which were used as typical biomarkers for BMSCs. The  
395 multi-lineage differentiation potential of BMSCs was detected, as shown in Fig.  
396 1B, BMSCs could be differentiated to osteoblasts, adipocytes and  
397 chondrocytes, which confirmed the stemness of BMSCs. Then, BMSCs were  
398 infected with lentiviral vectors carrying either the Cx43 gene combined with  
399 GFP or only GFP, and the stable transgenic Cx43-GFP-BMSCs and  
400 GFP-BMSCs cells were purified using puromycin for 5-6 days, and the results  
401 were confirmed by fluorescence (Fig. 1C). The expression of Cx43 was  
402 detected at both the mRNA and protein levels, which suggested that the cells  
403 were successfully transfected with the Cx43 gene (Fig. 1D-F).

404 Furthermore, Cx43 was greatly involved in cells proliferation and apoptosis.  
405 Therefore, we investigated these processes after Cx43 transfection. As  
406 depicted in Fig. 1G, Cx43 transfection in BMSCs had better results on reducing  
407 the inhibition effects of MPS on cells proliferation when compared with  
408 GFP-BMSCs or non-transfected cells. In addition, the apoptosis rate of cells  
409 was not significantly increased in the Cx43-GFP-BMSCs group compared with  
410 the GFP-BMSCs or non-transfection group under MPS treatment (Fig. 1H, 1I).

411

### 412 **Cx43 overexpression in BMSCs promotes angiogenesis and endothelial** 413 **cells recruitment in vitro**

414 Previous studies reported that Cx43 is greatly involved in the process of  
415 angiogenesis and endothelial cell recruitment. Therefore, Human umbilical  
416 cord vein endothelial cells (HUVECs) were used in this research to evaluate  
417 the tube formation activity of transgenic BMSCs. We found that the  
418 overexpression of Cx43 in BMSCs had resulted in a significantly higher tube  
419 formation ability than GFP-BMSCs or control groups (Fig. 2A-2C). After MPS  
420 treatment, which was used to mimic osteonecrosis in vitro, the tube formation  
421 ability was decreased (Fig. 2A-2C); However, Cx43 overexpression had  
422 significantly improved the tube formation ability compared with MPS treatment  
423 alone (Fig. 2A-2C). In addition, the expression of CD31, which is one of the

424 markers of angiogenesis, was detected, and HUVECs were cultured in the  
425 supernatants of Cx43-GFP-BMSCs, GFP-BMSCs or non-transfected cells for  
426 4 days. Results demonstrated that the expression of CD31 was significantly  
427 increased under the treatment of the Cx43-GFP-BMSCs supernatants in both  
428 the absence or presence conditions of MPS (Fig.2D, 2E).

429 Consistent with the results that were obtained in the tube formation assay,  
430 the supernatants of Cx43-GFP-BMSCs had significantly increased the  
431 migration ability of HUVECs cells, in a comparison with the supernatants of  
432 GFP-BMSCs or control groups, which was verified by wound-healing assay.  
433 MPS decreased the migration ability of HUVECs, and the supernatants of  
434 Cx43-GFP-BMSCs reversed these effects of MPS (Fig. 2F, 2G). In addition,  
435 the expression of MMP9, which is one of the markers of migration, was  
436 detected, and HUVECs were cultured in the supernatants of  
437 Cx43-GFP-BMSCs, GFP-BMSCs or non-transfected cells for 4 days. Results  
438 demonstrated that the expression of MMP9 was significantly increased under  
439 the treatment of the Cx43-GFP-BMSC supernatants in both the absence or  
440 presence conditions of MPS (Fig. 2H, 2I). Therefore, these results indicate that  
441 Cx43 overexpression could promote angiogenesis in vitro.

442

#### 443 **Osteogenic-associated proteins were up-regulated after Cx43** 444 **overexpression in BMSCs**

445 ALP staining was used to evaluate cells osteogenic differentiation, and the  
446 results showed that the osteogenic differentiation ability was obviously  
447 increased after transfected with Cx43-GFP-BMSCs in a comparison with the  
448 GFP-BMSCs and control groups in both the absence or presence conditions of  
449 MPS (Fig. 3A). Alizarin red staining indicated that more calcium nodules were  
450 observed in the Cx43-GFP-BMSCs group than in the GFP-BMSCs and control  
451 groups (Fig. 3B). Fewer calcium nodules were observed after induced by MPS;  
452 however, the number of calcium nodules was significantly increased in the  
453 group of Cx43 overexpressing in BMSCs under the treatment of MPS(Fig. 3B).

454 Osteogenic related proteins, including Runx2, ALP, Collagen I (COL I ) and  
455 OCN, play an essential role in the process of promoting osteogenesis. Our  
456 results showed that the protein expressions levels of Runx2, ALP, and COL I  
457 were significantly up-regulated in the Cx43 overexpression group at protein  
458 levels when compared with the GFP-BMSC group and the control group.  
459 Additionally, Dex could reduce the expressions of Runx2, ALP, and COL I ,  
460 while Cx43 overexpression in BMSCs had reversed the inhibition effects of  
461 MPS (Fig.3C-3F). Furthermore, the expressions levels of Runx2, ALP, COL I  
462 were also detected by immunofluorescence method, and the results were  
463 consistent with the western blot results (Fig 4). All the findings above showed  
464 that the Cx43 overexpression in BMSCs could facilitate the osteogenic  
465 differentiation in vitro.

466

#### 467 **Cx43 overexpression in BMSCs accelerates osteogenesis in a GIONFH** 468 **rat model**

469 To further study the role of Cx43 in ONFH in vivo, a rat model of GIONFH was  
470 successfully established and was identified by histomorphology as described  
471 previously. The results of H&E staining indicated that Cx43 overexpression in  
472 BMSCs reduced the morphological changes that were induced by MPS in vivo  
473 (Fig. 5A). In addition, our results demonstrated that BMSCs transplantation  
474 had partially promoted osteogenesis in GIONFH, whereas Cx43  
475 overexpression of BMSCs had significantly improved osteogenesis (Fig. 5B).  
476 The expressions levels of Runx2, ALP, COL I were decreased by MPS  
477 treatment at the protein level, and their expressions were rescued by the  
478 transplantation with Cx43 overexpression BMSCs in the femoral head tissues  
479 (Fig. 5C-5E). The presence of the transplanted BMSCs was confirmed by GFP  
480 immunohistochemical staining, and the results showed that the transgenic  
481 BMSCs were successfully located in the femoral head (Fig. 6A). The  
482 trabecular changes in the subchondral area of the femoral heads were  
483 visualized by micro-CT scanning. After eight weeks from the first MPS injection,



484 the occurrence rate of empty lacuna was significantly lower in the group of  
485 Cx43 overexpressing BMSCs transplantation than in GFP-BMSC group or  
486 control group (Fig. 6B). Furthermore, the BV/TV values were significantly  
487 decreased in the MPS group, whereas the Cx43 overexpression of BMSCs  
488 transplantation had significantly reduced the effect of MPS (Fig. 6C). In  
489 addition, the Tb. Th, and Tb. N, were remarkably improved after  
490 Cx43-GFP-BMSCs transplantation compared with the GFP-BMSCs group or  
491 MPS alone (Fig. 6D, 6E), however, Tb. Sp was significantly decreased after  
492 Cx43-GFP-BMSCs transplantation (Fig. 6F). All the results above indicated  
493 that Cx43 overexpression of BMSCs transplantation could decrease the  
494 osteonecrosis of GIONFH in vivo.

495

#### 496 **Cx43 overexpression promotes Angiogenesis**

497 Previous results suggested that Cx43 is greatly involved in the process of  
498 angiogenesis, and that is essential for osteogenesis. However, its function in  
499 the treatment for GIONFH in animal model is still not been investigated. We  
500 used angiography to visualize the angiogenesis process in vivo. As shown in  
501 **Fig. 7A**, MPS did not only impair the structure of the femoral head, but also  
502 destroyed the vascularization net around it. In the contrary, Cx43-GFP-BMSCs  
503 transplantation improved the angiogenesis and had significantly increased the  
504 volume of vessel in a comparison with the GFP-BMSCs and control groups.  
505 We have also found that the expression of VEGF and CD31 were significantly  
506 decreased in the MPS group, while both expressions levels were reversed in  
507 the Cx43-GFP-BMSCs transplantation group (Fig. 7B-7D). Therefore, Cx43  
508 overexpression in BMSCs could accelerate angiogenesis in a rat GIONFH  
509 model.

510

#### 511 **Discussion**

512 Numerous studies have found that there are a lot of factors and molecules that  
513 play an important role in BMSC-induced osteogenesis(16, 62), but the definite

514 basic mechanism still has not been explained clearly. We used lentiviral  
515 vectors to overexpression Cx43 in BMSCs and found that Cx43 promoted the  
516 efficacy of BMSC-induced bone formation by enhancing angiogenesis and  
517 osteogenesis. These results showed for the first time that Cx43 might be a vital  
518 potential therapeutic target against GIONFH.

519 Stem cell transplantation has been widely used in the treatment of various  
520 diseases, such as alteration of intestinal flora(28), diabetic neuropathy(13), and  
521 cardiac disease(34). However, satisfactory therapeutic effects are not always  
522 achieved by stem cells transplantation purely. Many studies have suggested  
523 that combining stem cells transplantation with genetic modification can  
524 improve the treatment efficiency of stem cell transplantation(3, 14, 26). BMSCs  
525 transplantation has been proved as a promising treatment method for the early  
526 stages of ONFH(10, 38, 52, 58). Previous studies demonstrated that SDF-1 $\alpha$   
527 overexpression could significantly promote bone regeneration through  
528 osteogenesis and angiogenesis(54), and the overexpression of P-glycoprotein  
529 or VEGF165 could also significantly decrease the incidence of GIONFH by  
530 promoting osteogenesis and blood vessel regeneration(16-17). In addition,  
531 Cx43 was found to be involved greatly in the process of osteogenesis and  
532 angiogenesis(35, 49). In this study, we found that Cx43 overexpression in  
533 BMSCs had significantly improved the osteogenic differentiation and HUVECs  
534 angiogenesis in vitro and promoted bone regeneration by osteogenesis and  
535 angiogenesis after cell transplantation in vivo. Our study provided evidence for  
536 the first time that Cx43 could promote BMSCs osteogenic differentiation and  
537 HUVECs angiogenesis during GIONFH treatment.

538 Runx2 is an osteogenesis signal molecular that plays an essential role in  
539 BMSCs osteogenic differentiation(22, 36). In our work, we found that Runx2  
540 expression was significantly decreased after MPS treatment, whereas the  
541 inhibition effects of MPS was attenuated after the overexpression of Cx43 in  
542 BMSCs. Lin F et al. reported that the knockdown of Cx43 expression could  
543 significantly decrease the osteogenic differentiation of BMSCs, which was

544 verified by the downregulation of Runx2, and this result is in consistent with our  
545 findings(32). Osteogenic differentiation of BMSCs is a key physiological  
546 process for bone formation, in which the Runx2 signal molecular is involved.  
547 **As shown in Fig. 3C**, we found that Cx43 overexpression could activate Runx2,  
548 which suggested that Cx43 could promote osteogenic differentiation in vitro.  
549 Furthermore, Micro-CT scanning and H&E staining, directly or indirectly,  
550 showed that Cx43 overexpression in BMSCs had significantly reversed  
551 MPS-induced osteonecrosis of the femoral head, and that bone trabecular  
552 parameters, including BV/TV, Tb. Th and Tb. N were significantly increased  
553 after Cx43-GFP-BMSCs transplantation. Therefore, transplantation with Cx43  
554 overexpressing BMSCs could accelerate bone regeneration in GIONFH  
555 treatment.

556 In addition to osteogenesis, BMSCs could also enhance the process of  
557 angiogenesis and blood vessel regeneration, which is essential for bone  
558 regeneration(37). Recent studies have shown that Cx43 can not only  
559 participates in cell migration, but also could promote angiogenesis in many  
560 kinds of tissues(11, 41, 46). In this study, we found that Cx43 overexpression in  
561 BMSCs could promoted tube formation and HUVECs migration in vitro. In  
562 addition, we furtherly confirmed that Cx43-GFP-BMSCs had significantly  
563 increased the vascularization and angiogenesis, as well as the volume of  
564 vessels, which were verified by angiography. All the results above suggested  
565 that Cx43 overexpression in BMSCs could promote BMSCs angiogenesis both  
566 in vitro and in vivo, indicating that Cx43 plays an essential role in the process  
567 of angiogenesis under the disease of ONFH.

568 In summary, our results indicate that Cx43 overexpression in BMSCs has good  
569 therapeutic effects on GIONFH by promoting angiogenesis and osteogenesis.  
570 Additionally, Cx43 is a potential therapeutic molecular for the treatment of  
571 GIONFH. However, further studies are still needed to investigate the function  
572 of Cx43 in larger animal models of GIONFH.

573

574 **Abbreviations**

575 BMSC: bone - marrow - derived mesenchymal stem cell; Cx43: connexin43; GIONFH:  
576 Glucocorticoid induced osteonecrosis of the femoral head; ALP: alkaline phosphatase;  
577 COL I : collagen type I ; FBS: fetal bovine serum; MPS: methylprednisolone; LPS:  
578 lipopolysaccharide; GFP: green fluorescent protein; HUVECs: human umbilical vein  
579 endothelial cells; DAPI: 4'6-diamidino-2-phenylindole; SD: standard deviation.

580

581 **Author Contributions**

582 X.Z., and C.C. performed the experiments, analyzed the data, and wrote the manuscript.  
583 Y.L. and D.L. carried out the experiments. Q.W. performed the data collection. P.K. and Y.F.  
584 study design, critical appraisal of manuscript. All authors approved the final version of the  
585 manuscript to be published.

586

587 **Author details**

588 <sup>1</sup>Department of Orthopaedics, Shandong Provincial Hospital Affiliated to Shandong First  
589 Medical University, Jinan 250021, People's Republic of China

590 <sup>2</sup>Department of Orthopaedics, West China Hospital, Sichuan University, No. 37 Wainan  
591 Guoxue Road, Chengdu 610041, People's Republic of China

592 <sup>3</sup>Pediatric Genetics, Shandong Maternal and Child Health Hospital, Jinan 250021,  
593 People's Republic of China

594

595 **Acknowledgements**

596 This work was supported by grants 81974333, 82172414 from the National Natural  
597 Science Foundation of China.

598

599 **Competing Interests**

600 The authors have declared that no competing interest exists.

601

602 **Availability of data and materials**

603 The data used to support the findings of this study are available from the corresponding

604 author upon request.

605

### 606 **Consent for publication**

607 All co-authors have read the manuscript and approved its submission to the Molecular  
608 and Cellular Biology.

609

### 610 **Ethics approval and consent to participate**

611 All animal experiments were performed based on the guidelines that are formulated by the  
612 National Institution of Health on the humane use and care of laboratory animals, and all  
613 animal protocols were approved by the Institutes Animal Care and Use Committee of  
614 West China Medical School of Sichuan University. This article does not contain any  
615 studies with patients who were performed by any of the authors.

616

### 617 **Funding**

618 This work was supported by grants 81974333, 82172414 from the National Natural  
619 Science Foundation of China.

## 620 **References**

621

- 622 1. Aasen, T., E. Leithe, S.V. Graham, P. Kameritsch, M.D. Mayán, M. Mesnil, K. Pogoda, and A. Tabernero.  
623 2019. Connexins in cancer: bridging the gap to the clinic. *Oncogene*. **38**:4429-4451.
- 624 2. Bennett, M.V., J.M. Garré, J.A. Orellana, F.F. Bukauskas, M. Nedergaard, and J.C. Sáez. 2012. Connexin  
625 and pannexin hemichannels in inflammatory responses of glia and neurons. *Brain Res.* **1487**:3-15.
- 626 3. Bortolomai, I., M. Sandri, E. Draghici, E. Fontana, E. Campodoni, G.E. Marcovecchio, F. Ferrua, L.  
627 Perani, A. Spinelli, T. Canu, M. Catucci, T. Di Tomaso, L. Sergi Sergi, A. Esposito, A. Lombardo, L.  
628 Naldini, A. Tampieri, G.A. Hollander, A. Villa, and M. Bosticardo. 2019. Gene Modification and  
629 Three-Dimensional Scaffolds as Novel Tools to Allow the Use of Postnatal Thymic Epithelial Cells for  
630 Thymus Regeneration Approaches. *Stem Cells Transl Med*. **8**:1107-1122.
- 631 4. Cao, Y., J. Xiong, S. Mei, F. Wang, Z. Zhao, S. Wang, and Y. Liu. 2015. Aspirin promotes bone marrow  
632 mesenchymal stem cell-based calvarial bone regeneration in mini swine. *Stem Cell Res Ther*. **6**:210.
- 633 5. Chuah, Y.J., J.R. Tan, Y. Wu, C.S. Lim, H.T. Hee, Y. Kang, and D.A. Wang. 2020. Scaffold-free tissue  
634 engineering with aligned bone marrow stromal cell sheets to recapitulate the microstructural and  
635 biochemical composition of annulus fibrosus. *Acta Biomater*. **107**:129-137.
- 636 6. Coutinho, A.E., and K.E. Chapman. 2011. The anti-inflammatory and immunosuppressive effects of  
637 glucocorticoids, recent developments and mechanistic insights. *Mol. Cell. Endocrinol.* **335**:2-13.
- 638 7. Czyż, J., K. Piwarczyk, M. Paw, M. Luty, T. Wróbel, J. Catapano, Z. Madeja, and D. Ryszawy. 2017.  
639 Connexin-dependent intercellular stress signaling in tissue homeostasis and tumor development. *Acta*

- 640 biochimica Polonica. **64**:377-389.
- 641 8.**Ding, P., W. Zhang, Q. Tan, C. Yao, and S. Lin.** 2019. Impairment of circulating endothelial progenitor cells  
642 (EPCs) in patients with glucocorticoid-induced avascular necrosis of the femoral head and changes of  
643 EPCs after glucocorticoid treatment in vitro. *J Orthop Surg Res.* **14**:226.
- 644 9.**Ding, Z., and H. Huang.** 2015. Mesenchymal stem cells in rabbit meniscus and bone marrow exhibit a similar  
645 feature but a heterogeneous multi-differentiation potential: superiority of meniscus as a cell source for  
646 meniscus repair. *BMC Musculoskelet Disord.* **16**:65.
- 647 10.**Döring, M., T. Kluba, K.M. Cabanillas Stanchi, P. Kahle, K. Lenglinger, I. Tsifikas, C. Treuner, M.**  
648 **Vaegler, M. Mezger, A. Erbacher, M. Schumm, P. Lang, R. Handgretinger, and I. Müller.** 2020.  
649 Longtime Outcome After Intraosseous Application of Autologous Mesenchymal Stromal Cells in Pediatric  
650 Patients and Young Adults with Avascular Necrosis After Steroid or Chemotherapy. *Stem Cells Dev.* .
- 651 11.**Fan, X., Y. Teng, Z. Ye, Y. Zhou, and W.S. Tan.** 2018. The effect of gap junction-mediated transfer of  
652 miR-200b on osteogenesis and angiogenesis in a co-culture of MSCs and HUVECs. *J. Cell. Sci.* **131**.
- 653 12.**Gangji, V., V. De Maertelaer, and J.P. Hauzeur.** 2011. Autologous bone marrow cell implantation in the  
654 treatment of non-traumatic osteonecrosis of the femoral head: Five year follow-up of a prospective  
655 controlled study. *Bone.* **49**:1005-1009.
- 656 13.**Gur, S., and W. Hellstrom.** 2019. Harnessing Stem Cell Potential for the Treatment of Erectile Function with  
657 Diabetes Mellitus: From Preclinical/Clinical Perspectives to Penile Tissue Engineering. *Curr Stem Cell Res*  
658 *Ther.* .
- 659 14.**Hamed, E.M., M.H. Meabed, U.F. Aly, and R. Hussein.** 2019. Recent Progress in Gene Therapy and Other  
660 Targeted Therapeutic Approaches for Beta Thalassemia. *Curr Drug Targets.* **20**:1603-1623.
- 661 15.**Han, L., B. Wang, R. Wang, S. Gong, G. Chen, and W. Xu.** 2019. The shift in the balance between  
662 osteoblastogenesis and adipogenesis of mesenchymal stem cells mediated by glucocorticoid receptor. *Stem*  
663 *Cell Res Ther.* **10**:377.
- 664 16.**Han, N., Z. Li, Z. Cai, Z. Yan, Y. Hua, and C. Xu.** 2016. P-glycoprotein overexpression in bone  
665 marrow-derived multipotent stromal cells decreases the risk of steroid-induced osteonecrosis in the femoral  
666 head. *J. Cell. Mol. Med.* **20**:2173-2182.
- 667 17.**Hang, D., Q. Wang, C. Guo, Z. Chen, and Z. Yan.** 2012. Treatment of osteonecrosis of the femoral head with  
668 VEGF165 transgenic bone marrow mesenchymal stem cells in mongrel dogs. *Cells Tissues Organs (Print).*  
669 **195**:495-506.
- 670 18.**Hashimoto, Y., Y. Nishida, S. Takahashi, H. Nakamura, H. Mera, K. Kashiwa, S. Yoshiya, Y. Inagaki, K.**  
671 **Uematsu, Y. Tanaka, S. Asada, M. Akagi, K. Fukuda, Y. Hosokawa, A. Myoui, N. Kamei, M. Ishikawa,**  
672 **N. Adachi, M. Ochi, and S. Wakitani.** 2019. Transplantation of autologous bone marrow-derived  
673 mesenchymal stem cells under arthroscopic surgery with microfracture versus microfracture alone for  
674 articular cartilage lesions in the knee: A multicenter prospective randomized control clinical trial. *Regen*  
675 *Ther.* **11**:106-113.
- 676 19.**Hernigou, P., A. Dubory, C.H. Flouzat Lachaniette, I. Khaled, N. Chevallier, and H. Rouard.** 2018. Stem  
677 cell therapy in early post-traumatic talus osteonecrosis. *Int Orthop.* **42**:2949-2956.
- 678 20.**Hernigou, P., M. Trousselier, F. Roubineau, C. Bouthors, N. Chevallier, H. Rouard, and C.H.**  
679 **Flouzat-Lachaniette.** 2016. Stem Cell Therapy for the Treatment of Hip Osteonecrosis: A 30-Year Review  
680 of Progress. *Clin Orthop Surg.* **8**:1-8.
- 681 21.**Hu, Y., S.S. Rao, Z.X. Wang, J. Cao, Y.J. Tan, J. Luo, H.M. Li, W.S. Zhang, C.Y. Chen, and H. Xie.** 2018.  
682 Exosomes from human umbilical cord blood accelerate cutaneous wound healing through  
683 miR-21-3p-mediated promotion of angiogenesis and fibroblast function. *Theranostics.* **8**:169-184.

- 684 22.**Jiang, H.T., C.C. Ran, Y.P. Liao, J.H. Zhu, H. Wang, R. Deng, M. Nie, B.C. He, and Z.L. Deng.** 2019.  
685 IGF-1 reverses the osteogenic inhibitory effect of dexamethasone on BMP9-induced osteogenic  
686 differentiation in mouse embryonic fibroblasts via PI3K/AKT/COX-2 pathway. *J. Steroid Biochem. Mol.*  
687 *Biol.* **191**:105363.
- 688 23.**Jiang, J.X., A.J. Siller-Jackson, and S. Burra.** 2007. Roles of gap junctions and hemichannels in bone cell  
689 functions and in signal transmission of mechanical stress. *Front. Biosci.* **12**:1450-1462.
- 690 24.**Kang, J.S., K.H. Moon, B.S. Kim, D.G. Kwon, S.H. Shin, B.K. Shin, and D.J. Ryu.** 2013. Clinical results of  
691 auto-iliac cancellous bone grafts combined with implantation of autologous bone marrow cells for  
692 osteonecrosis of the femoral head: a minimum 5-year follow-up. *Yonsei Med. J.* **54**:510-515.
- 693 25.**Kar, R., N. Batra, M.A. Riquelme, and J.X. Jiang.** 2012. Biological role of connexin intercellular channels  
694 and hemichannels. *Arch. Biochem. Biophys.* **524**:2-15.
- 695 26.**Korshunova, I., S. Rhein, D. García-González, I. Stölting, U. Pfisterer, A. Barta, O. Dmytriyeva, A.**  
696 **Kirkeby, M. Schwaninger, and K. Khodosevich.** 2020. Genetic modification increases the survival and  
697 the neuroregenerative properties of transplanted neural stem cells. *JCI Insight* **5**.
- 698 27.**Kubo, T., K. Ueshima, M. Saito, M. Ishida, Y. Arai, and H. Fujiwara.** 2016. Clinical and basic research on  
699 steroid-induced osteonecrosis of the femoral head in Japan. *J Orthop Sci.* **21**:407-413.
- 700 28.**Kusakabe, S., K. Fukushima, T. Maeda, D. Motooka, S. Nakamura, J. Fujita, T. Yokota, H. Shibayama,**  
701 **K. Oritani, and Y. Kanakura.** 2020. Pre- and post-serial metagenomic analysis of gut microbiota as a  
702 prognostic factor in patients undergoing haematopoietic stem cell transplantation. *Br. J. Haematol.*  
703 **188**:438-449.
- 704 29.**Leithe, E., M. Mesnil, and T. Aasen.** 2018. The connexin 43 C-terminus: A tail of many tales. *Biochim*  
705 *Biophys Acta Biomembr.* **1860**:48-64.
- 706 30.**Li, J., Q. Shao, X. Zhu, and G. Sun.** 2020. Efficacy of autologous bone marrow mesenchymal stem cells in the  
707 treatment of knee osteoarthritis and their effects on the expression of serum TNF- $\alpha$  and IL-6. *J*  
708 *Musculoskelet Neuronal Interact.* **20**:128-135.
- 709 31.**Li, S., H. Zhang, S. Li, Y. Yang, B. Huo, and D. Zhang.** 2015. Connexin 43 and ERK regulate  
710 tension-induced signal transduction in human periodontal ligament fibroblasts. *J. Orthop. Res.*  
711 **33**:1008-1014.
- 712 32.**Lin, F.X., G.Z. Zheng, B. Chang, R.C. Chen, Q.H. Zhang, P. Xie, D. Xie, G.Y. Yu, Q.X. Hu, D.Z. Liu, S.X.**  
713 **Du, and X.D. Li.** 2018. Connexin 43 Modulates Osteogenic Differentiation of Bone Marrow Stromal Cells  
714 Through GSK-3 $\beta$ /Beta-Catenin Signaling Pathways. *Cell. Physiol. Biochem.* **47**:161-175.
- 715 33.**Liu, D., Y. Yang, F. Kuang, S. Qing, B. Hu, and X. Yu.** 2019. Risk of infection with different  
716 immunosuppressive drugs combined with glucocorticoids for the treatment of idiopathic membranous  
717 nephropathy: A pairwise and network meta-analysis. *Int. Immunopharmacol.* **70**:354-361.
- 718 34.**Liu, Y., R. Niu, W. Li, J. Lin, C. Stamm, G. Steinhoff, and N. Ma.** 2019. Therapeutic potential of menstrual  
719 blood-derived endometrial stem cells in cardiac diseases. *Cell. Mol. Life Sci.* **76**:1681-1695.
- 720 35.**Moorer, M.C., and J.P. Stains.** 2017. Connexin43 and the Intercellular Signaling Network Regulating Skeletal  
721 Remodeling. *Curr Osteoporos Rep.* **15**:24-31.
- 722 36.**Nagel, A.K., and L.E. Ball.** 2014. O-GlcNAc modification of the runt-related transcription factor 2 (Runx2)  
723 links osteogenesis and nutrient metabolism in bone marrow mesenchymal stem cells. *Mol. Cell Proteomics.*  
724 **13**:3381-3395.
- 725 37.**Nguyen, V.T., B. Canciani, F. Cirillo, L. Anastasia, G.M. Peretti, and L. Mangiavini.** 2020. Effect of  
726 Chemically Induced Hypoxia on Osteogenic and Angiogenic Differentiation of Bone Marrow  
727 Mesenchymal Stem Cells and Human Umbilical Vein Endothelial Cells in Direct Coculture. *Cells.* **9**.



- 728 38.**Pan, J., Q. Ding, S. Lv, B. Xia, H. Jin, D. Chen, L. Xiao, and P. Tong.** 2020. Prognosis after autologous  
729 peripheral blood stem cell transplantation for osteonecrosis of the femoral head in the pre-collapse stage: a  
730 retrospective cohort study. *Stem Cell Res Ther.* **11**:83.
- 731 39.**Peng, W.X., and L. Wang.** 2017. Adenovirus-Mediated Expression of BMP-2 and BFGF in Bone Marrow  
732 Mesenchymal Stem Cells Combined with Demineralized Bone Matrix For Repair of Femoral Head  
733 Osteonecrosis in Beagle Dogs. *Cell. Physiol. Biochem.* **43**:1648-1662.
- 734 40.**Plotkin, L.I., D.W. Laird, and J. Amedee.** 2016. Role of connexins and pannexins during ontogeny,  
735 regeneration, and pathologies of bone. *BMC Cell Biol.* **17 Suppl 1**:19.
- 736 41.**Pohl, U.** 2020. Connexins: Key Players in the Control of Vascular Plasticity and Function. *Physiol. Rev.*  
737 **100**:525-572.
- 738 42.**Rubessa, M., K. Polkoff, M. Bionaz, E. Monaco, D.J. Milner, S.J. Hollister, M.S. Goldwasser, and M.B.**  
739 **Wheeler.** 2017. Use of Pig as a Model for Mesenchymal Stem Cell Therapies for Bone Regeneration.  
740 *Anim. Biotechnol.* **28**:275-287.
- 741 43.**Schepper, J.D., F. Collins, N.D. Rios-Arce, H.J. Kang, L. Schaefer, J.D. Gardinier, R. Raghuvanshi, R.A.**  
742 **Quinn, R. Britton, N. Parameswaran, and L.R. McCabe.** 2020. Involvement of the Gut Microbiota and  
743 Barrier Function in Glucocorticoid-Induced Osteoporosis. *J. Bone Miner. Res.* **35**:801-820.
- 744 44.**Shen, C., M.R. Kim, J.M. Noh, S.J. Kim, S.O. Ka, J.H. Kim, B.H. Park, and J.H. Park.** 2016.  
745 Glucocorticoid Suppresses Connexin 43 Expression by Inhibiting the Akt/mTOR Signaling Pathway in  
746 Osteoblasts. *Calcif. Tissue Int.* **99**:88-97.
- 747 45.**Singh, J.A., A. Hossain, A. Kotb, and G. Wells.** 2016. Risk of serious infections with immunosuppressive  
748 drugs and glucocorticoids for lupus nephritis: a systematic review and network meta-analysis. *BMC Med.*  
749 **14**:137.
- 750 46.**Slavi, N., A.H. Toychiev, S. Kosmidis, J. Ackert, S.A. Bloomfield, H. Wulff, S. Viswanathan, P.D. Lampe,**  
751 **and M. Srinivas.** 2018. Suppression of connexin 43 phosphorylation promotes astrocyte survival and  
752 vascular regeneration in proliferative retinopathy. *Proc. Natl. Acad. Sci. U.S.A.* **115**:E5934-5934E5943.
- 753 47.**Slominski, R.M., R.C. Tuckey, P.R. Manna, A.M. Jetten, A. Postlethwaite, C. Raman, and A.T. Slominski.**  
754 2020. Extra-adrenal glucocorticoid biosynthesis: implications for autoimmune and inflammatory disorders.  
755 *Genes Immun.* .
- 756 48.**Tao, S.C., T. Yuan, B.Y. Rui, Z.Z. Zhu, S.C. Guo, and C.Q. Zhang.** 2017. Exosomes derived from human  
757 platelet-rich plasma prevent apoptosis induced by glucocorticoid-associated endoplasmic reticulum stress  
758 in rat osteonecrosis of the femoral head via the Akt/Bad/Bcl-2 signal pathway. *Theranostics.* **7**:733-750.
- 759 49.**Wang, D.G., F.X. Zhang, M.L. Chen, H.J. Zhu, B. Yang, and K.J. Cao.** 2014. Cx43 in mesenchymal stem  
760 cells promotes angiogenesis of the infarcted heart independent of gap junctions. *Mol Med Rep.*  
761 **9**:1095-1102.
- 762 50.**Wang, H.H., C.H. Su, Y.J. Wu, J.Y. Li, Y.M. Tseng, Y.C. Lin, C.L. Hsieh, C.H. Tsai, and H.I. Yeh.** 2013.  
763 Reduction of connexin43 in human endothelial progenitor cells impairs the angiogenic potential.  
764 *Angiogenesis.* **16**:553-560.
- 765 51.**Wang, K., J. Li, Z. Li, B. Wang, Y. Qin, N. Zhang, H. Zhang, X. Su, Y. Wang, and H. Zhu.** 2019.  
766 Chondrogenic Progenitor Cells Exhibit Superiority Over Mesenchymal Stem Cells and Chondrocytes in  
767 Platelet-Rich Plasma Scaffold-Based Cartilage Regeneration. *Am J Sports Med.* **47**:2200-2215.
- 768 52.**Wu, Z.Y., Q. Sun, M. Liu, B.E. Grottkau, Z.X. He, Q. Zou, and C. Ye.** 2020. Correlation between the  
769 efficacy of stem cell therapy for osteonecrosis of the femoral head and cell viability. *BMC Musculoskelet*  
770 *Disord.* **21**:55.
- 771 53.**Xu, S., R. Guo, P.Z. Li, K. Li, Y. Yan, J. Chen, G. Wang, B. Brand-Saberi, X. Yang, and X. Cheng.** 2019.



- 772 Dexamethasone interferes with osteoblasts formation during osteogenesis through altering IGF-1-mediated  
773 angiogenesis. *J. Cell. Physiol.* .
- 774 54. **Yang, F., F. Xue, J. Guan, Z. Zhang, J. Yin, and Q. Kang.** 2018. Stromal-Cell-Derived Factor (SDF) 1-Alpha  
775 Overexpression Promotes Bone Regeneration by Osteogenesis and Angiogenesis in Osteonecrosis of the  
776 Femoral Head. *Cell. Physiol. Biochem.* **46**:2561-2575.
- 777 55. **Yu, H., P. Liu, W. Zuo, X. Sun, H. Liu, F. Lu, W. Guo, and Q. Zhang.** 2020. Decreased angiogenic and  
778 increased apoptotic activities of bone microvascular endothelial cells in patients with  
779 glucocorticoid-induced osteonecrosis of the femoral head. *BMC Musculoskelet Disord.* **21**:277.
- 780 56. **Zha, X., B. Sun, R. Zhang, C. Li, Z. Yan, and J. Chen.** 2018. Regulatory effect of microRNA-34a on  
781 osteogenesis and angiogenesis in glucocorticoid-induced osteonecrosis of the femoral head. *J. Orthop. Res.*  
782 **36**:417-424.
- 783 57. **Zhao, D., D. Cui, B. Wang, F. Tian, L. Guo, L. Yang, B. Liu, and X. Yu.** 2012. Treatment of early stage  
784 osteonecrosis of the femoral head with autologous implantation of bone marrow-derived and cultured  
785 mesenchymal stem cells. *Bone.* **50**:325-330.
- 786 58. **Zhao, D., Y. Liu, C. Ma, G. Gu, and D.F. Han.** 2019. A Mini Review: Stem Cell Therapy for Osteonecrosis of  
787 the Femoral Head and Pharmacological Aspects. *Curr. Pharm. Des.* **25**:1099-1104.
- 788 59. **Zhao, L., S. Jiang, and B.M. Hantash.** 2010. Transforming growth factor beta1 induces osteogenic  
789 differentiation of murine bone marrow stromal cells. *Tissue Eng Part A.* **16**:725-733.
- 790 60. **Zhao, X., X.W. Wang, K.S. Zhou, W. Nan, Y.Q. Guo, J.L. Kou, J. Wang, Y.Y. Xia, and H.H. Zhang.** 2017.  
791 Expression of Ski and its role in astrocyte proliferation and migration. *Neuroscience.* **362**:1-12.
- 792 61. **Zhao, X., Z. Wei, D. Li, Z. Yang, M. Tian, and P. Kang.** 2019. Glucocorticoid Enhanced the Expression of  
793 Ski in Osteonecrosis of Femoral Head: The Effect on Adipogenesis of Rabbit BMSCs. *Calcif. Tissue Int.*  
794 **105**:506-517.
- 795 62. **Zhou, D., Y.X. Chen, J.H. Yin, S.C. Tao, S.C. Guo, Z.Y. Wei, Y. Feng, and C.Q. Zhang.** 2018. Valproic acid  
796 prevents glucocorticoid-induced osteonecrosis of the femoral head of rats. *Int. J. Mol. Med.* **41**:3433-3447.
- 797 63. **Zhun, W., L. Donghai, Y. Zhouyuan, Z. Haiyan, and K. Pengde.** 2018. Efficiency of Cell Therapy to  
798 GC-Induced ONFH: BMSCs with Dkk-1 Interference Is Not Superior to Unmodified BMSCs. *Stem Cells*  
799 *Int.* **2018**:1340252.

800

801

802

803

804

805

806

807

808

809

810

811 **Figure 1. Characteristics of isolated rats' bone marrow stromal stem cells**

812 (BMSCs) and transfection efficacy evaluation. (A) The isolated BMSCs were  
813 positive for CD29 and CD90, but negative for CD45 and CD34. The X axis  
814 represents fluorescence intensity; (B) BMSCs were differentiated to  
815 osteoblasts, adipocytes and chondrocytes; (C) BMSCs were successfully  
816 transfected with lentiviral vectors, as indicated by fluorescence; (D) The  
817 expression of Cx43 mRNA was detected by RT-PCR; (E) After transfected  
818 with the Cx43 gene, the protein expression level of Cx43 was detected by  
819 Western blot; (F) Statistical analysis for Cx43 expression; (G) The effects of  
820 Lv-Cx43 on BMSCs proliferation. (H) The effects of Lv-Cx43 on BMSCs  
821 apoptosis measured by flow cytometry, Q2-UL represents necrotic cells,  
822 Q2-UR represents late apoptotic cells, Q2-LR represents early apoptotic cells  
823 and Q2-LL represents live cells; (I) Statistical analysis of apoptosis. Each  
824 experiment was repeatedly performed at least three times. \*P<0.05.

825

826 Figure 2. Cx43 overexpression in BMSCs promotes angiogenesis in vitro. (A)  
827 Cell supernatants of Cx43-GFP-BMSCs had significantly promoted tube  
828 formation compared with GFP-BMSCs or control groups. Tube formation was  
829 reduced by MPS, but Cx43 overexpression reversed the effects that were  
830 caused by MPS. (B-C) The finding of the changes of total tube length and total  
831 branching points were in line with the results that were observed for tube  
832 formation. (D) HUVECs were cultured in the supernatants of  
833 Cx43-GFP-BMSCs, GFP-BMSCs or non-transfected cells for 4 days, and the  
834 expression level for CD31 was detected by Western blot. (E) Statistical  
835 analysis of CD31 expression. (F) The supernatants of Cx43-GFP-BMSCs had  
836 significantly promoted HUVECs' migration compared with the GFP-BMSCs or  
837 control groups. HUVECs' migration ability was decreased by MPS treatment,  
838 whereas Cx43 overexpression reversed the effects that were caused by MPS;  
839 (G) Statistical analysis for all the groups of cells migration. (H) The expression  
840 of MMP9 in HUVECs was measured by western blot analysis. (I) Statistical  
841 analysis for MMP9 expression; Each experiment was repeatedly performed at

842 least three times. \*P<0.05.

843

844 Figure 3. Cx43 overexpression had significantly promoted calcium nodules  
845 formation and the expression of osteogenic-related proteins in BMSCs in vitro.

846 (A) The expression of ALP was determined by ALP staining. ALP expression  
847 was significantly increased in the Cx43-GFP-BMSCs group, and the ALP  
848 expression that was decreased by MPS was reversed by Cx43 overexpression  
849 in BMSCs. (B) Cx43-GFP-BMSCs induced the formation of a higher number of  
850 calcium nodules than that in the GFP-BMSCs, which was identified by Alizarin  
851 red staining. The number of calcium nodules was decreased by MPS and was  
852 obviously reversed by Cx43 overexpression in BMSCs. (C) The expressions  
853 levels of osteogenic-related proteins, including Runx2, ALP, and COL I were  
854 upregulated at the protein level in BMSCs after Cx43 overexpression. MPS  
855 decreased the expressions of Runx2, ALP, and COL I , and their expressions  
856 were restored by Cx43 overexpression. (D) Statistical analysis for Runx2  
857 expression. (E) Statistical analysis for ALP expression. (F) Statistical analysis  
858 for COL I expression; Each experiment was performed repeatedly at least  
859 three times. \*P<0.05.

860

861 Figure 4. Immunofluorescence staining analysis about the expression of Cx43,  
862 Runx2, ALP, and COL I in normal or transfected BMSCs treated or untreated  
863 with MPS. (A) Double immunofluorescence staining of Cx43 (red) and DAPI  
864 (blue); (B) Double immunofluorescence staining of Runx2 (red) and DAPI  
865 (blue); (C) Double immunofluorescence staining of ALP (red) and DAPI (blue);  
866 (D) Double immunofluorescence staining of COL I (red) and DAPI (blue).  
867 Magnified area in the frame showed that the fluorescence intensity of Cx43,  
868 Runx2, ALP and COL I were significantly increased in the Cx43-GFP-BMSCs  
869 group, and all of the above indexes of fluorescence intensity were decreased  
870 by MPS, which were reversed by Cx43 overexpression in BMSCs. Images are  
871 representatives of at least three experiments.

872

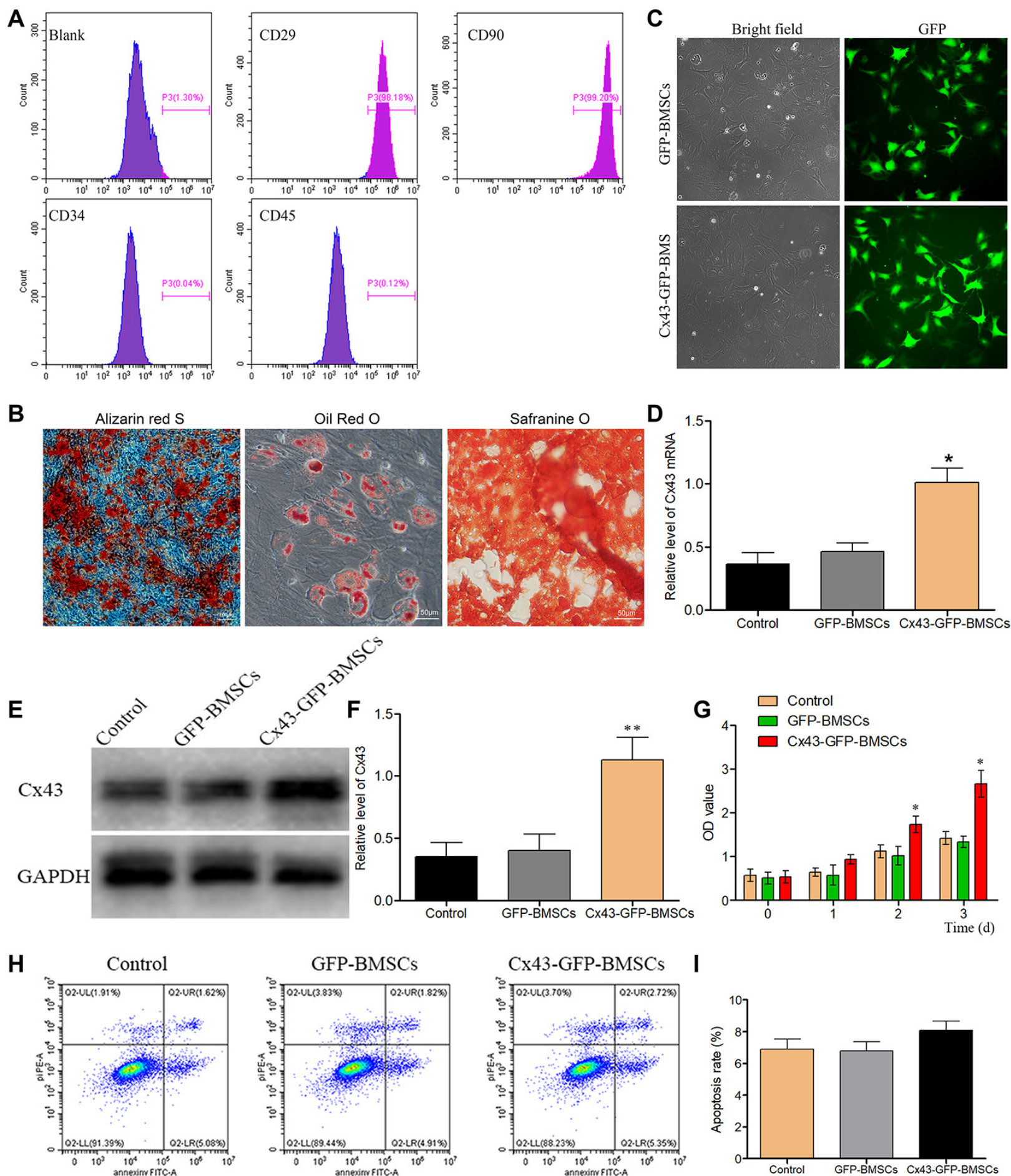
873 Figure 5. Cx43-GFP-BMSCs promote osteogenesis in vivo. (A) The  
874 overexpression of Cx43 in BMSCs reduced the morphological changes that  
875 were induced by MPS as indicated by H&E staining. Arrow indicates empty  
876 lacunae. (B) Cx43-GFP-BMSCs promoted the expression of Runx2, ALP and  
877 COL I despite the presence of MPS. Arrows indicate the expressions of  
878 Runx2, ALP and COL I. (C) Density evaluation of Runx2. (D) Density  
879 evaluation of ALP. (E) Density evaluation of COL. Each experiment was  
880 repeated performed at least three times. \*P<0.05.

881

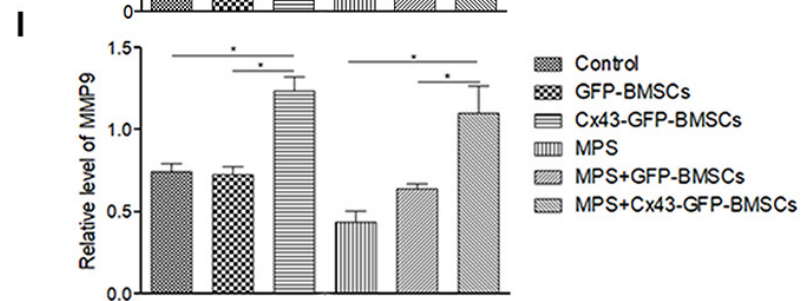
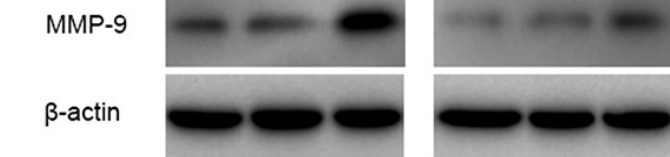
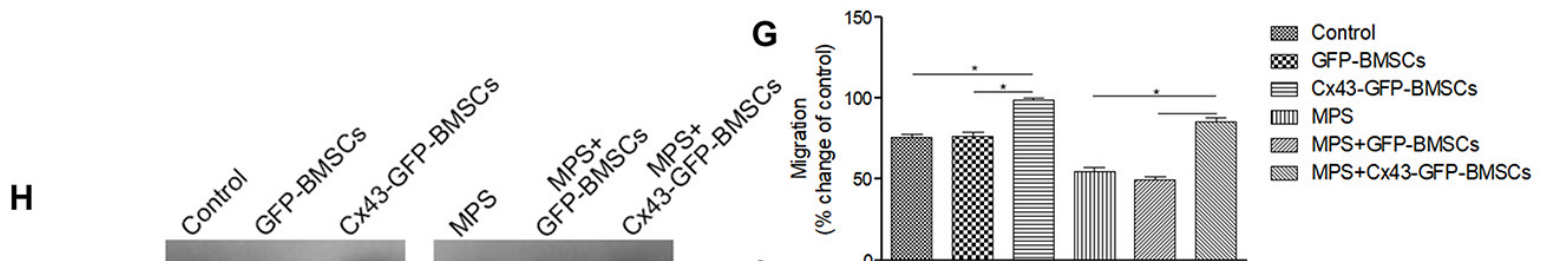
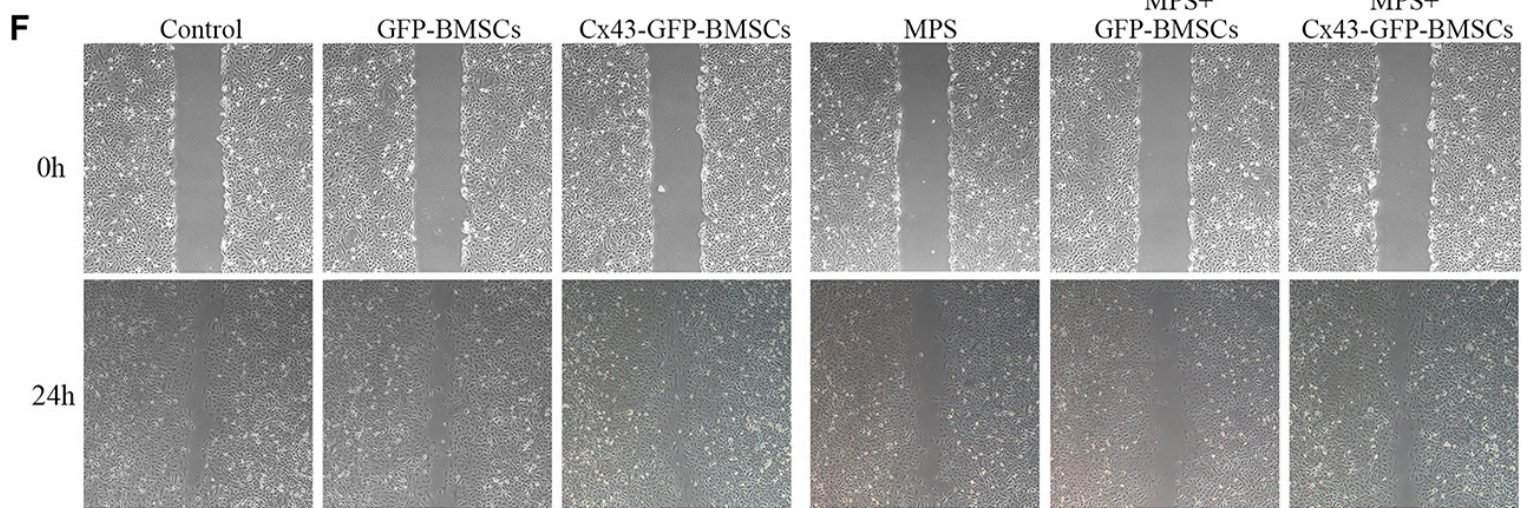
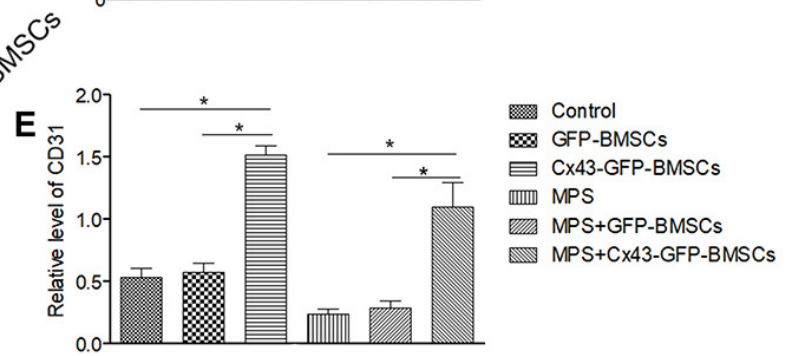
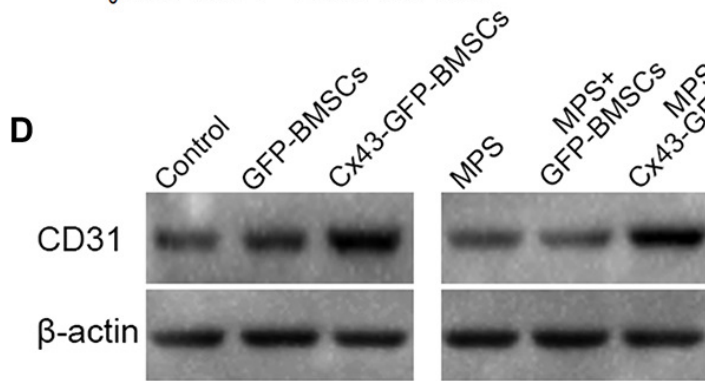
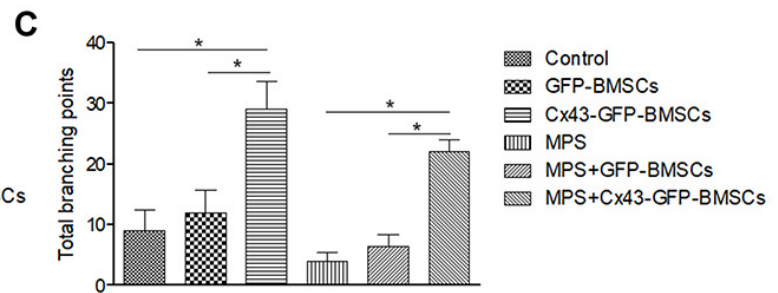
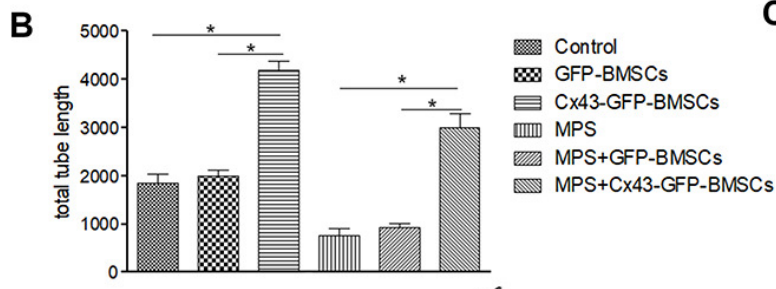
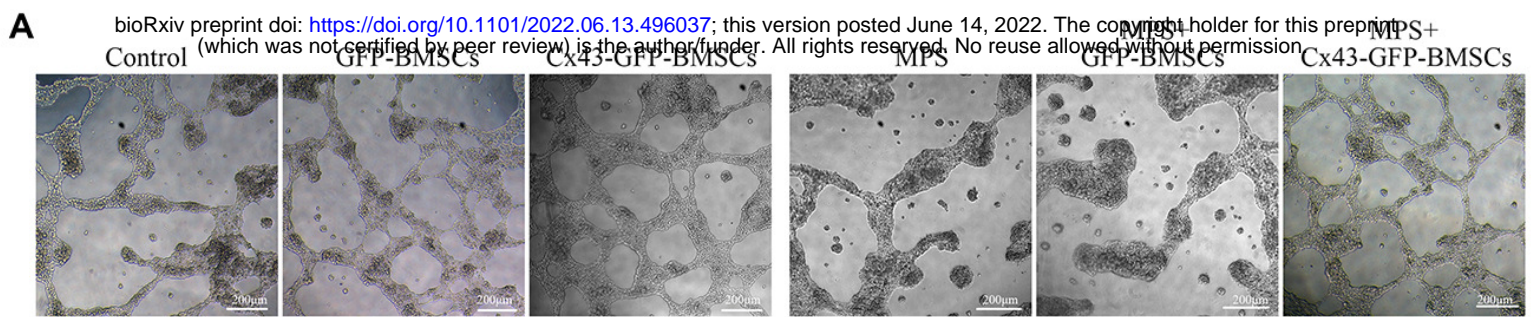
882 Figure 6. Cx43-GFP-BMSCs promote angiogenesis in vivo. (A) Cx43  
883 overexpression in BMSCs promote vascularization, as indicated by  
884 angiography. Arrows indicate vessels in the bones. (B-C) Quantitative analysis  
885 of the vascularized area in the femoral head receiving different treatment. (D)  
886 The expression of the angiogenesis indicator VEGF and CD31 were  
887 upregulated by Cx43-GFP-BMSCs despite the presence of MPS. Arrow  
888 indicates the expression of VEGF and CD31; (E) Density evaluation of VEGF;  
889 (F) Density evaluation of CD31. Each experiment was repeated performed at  
890 least three times. \*P<0.05.

891

892 Figure 7. Cx43-GFP-BMSCs promote osteogenesis as indicated by trabecular  
893 bone parameters. (A) Immunohistochemistry staining for GFP indicated that  
894 the transgenic BMSCs were located in the femoral head. Arrows indicate the  
895 localization of GFP-labeled BMSCs. (B) Direct visualization of the  
896 morphological changes: Cx43-GFP-BMSCs reversed MPS-induced  
897 osteonecrosis. (C-F) Changes of the trabecular bone parameters: bone  
898 volume per tissue volume (BV/TV); trabecular thickness (Tb. Th); and  
899 trabecular number (Tb. N); trabecular separation (Tb.Sp). Each experiment  
900 was repeated performed at least three times. \*P<0.05.

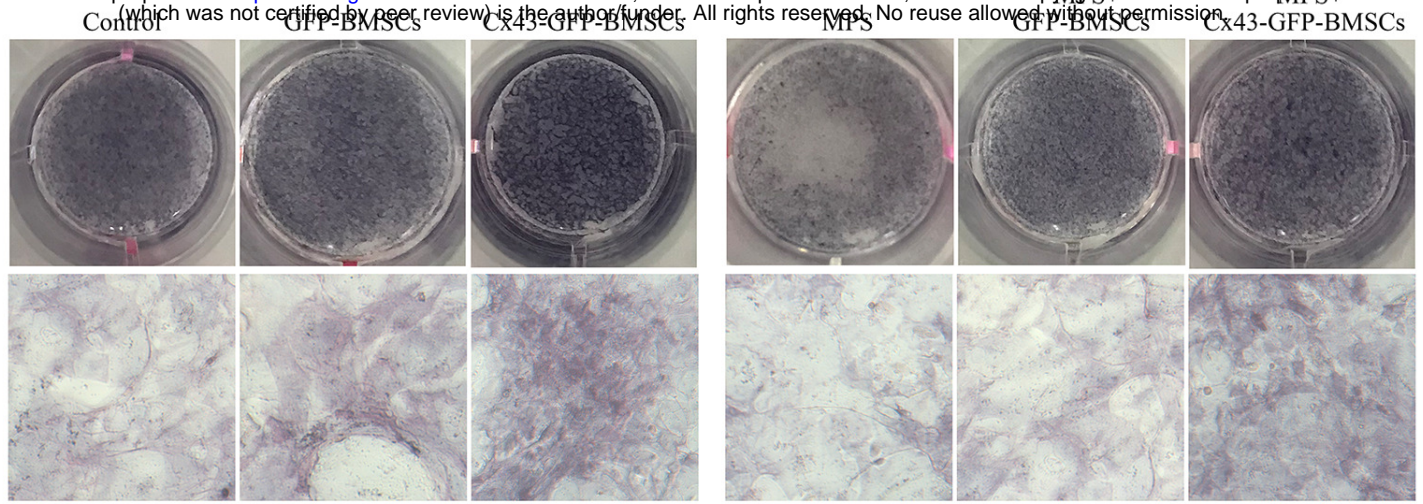




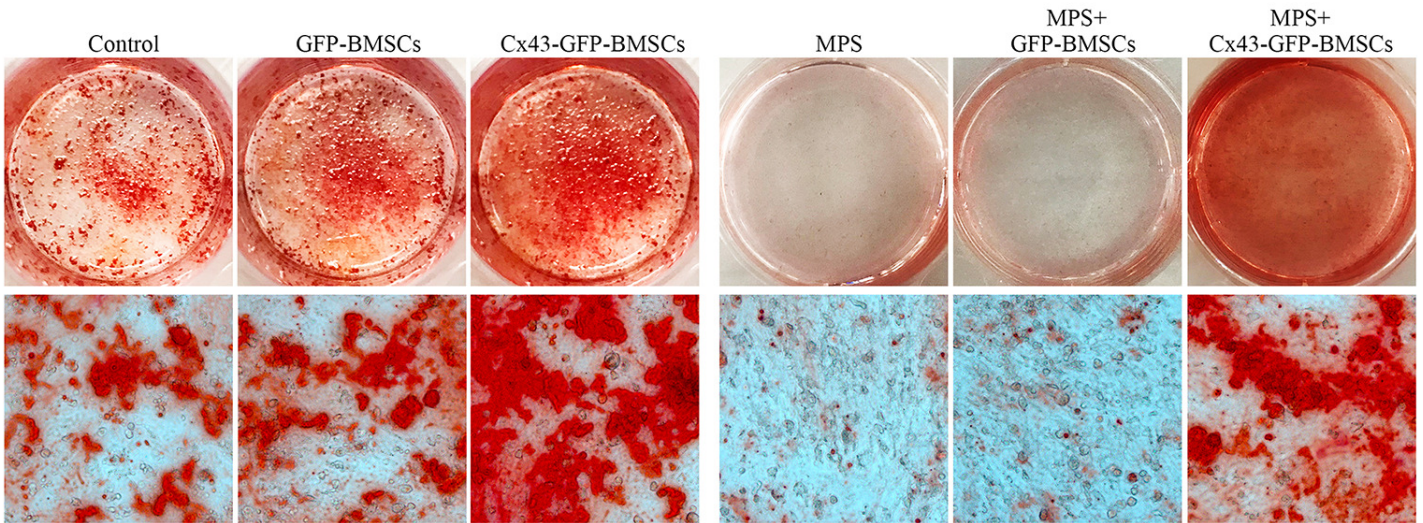




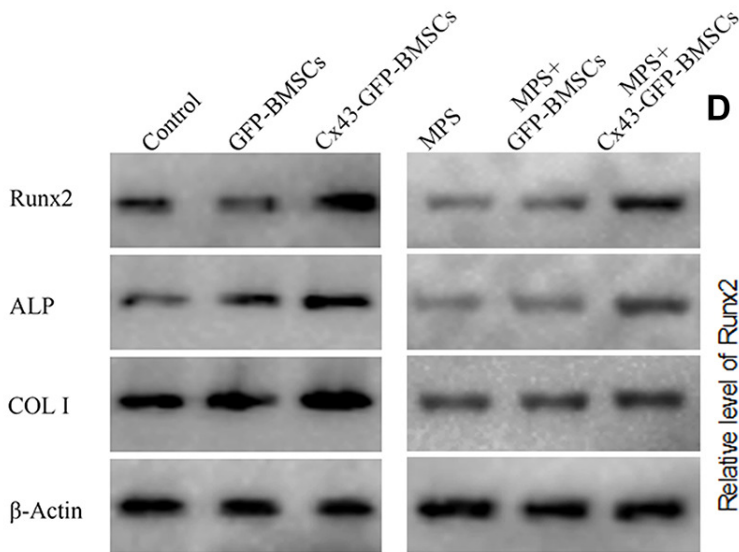
**A**



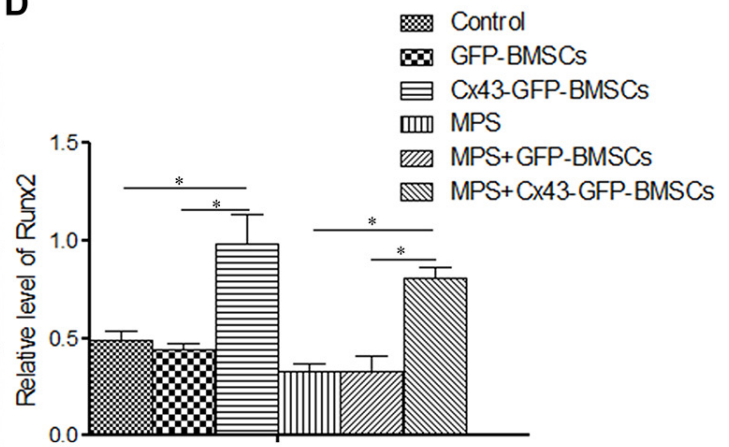
**B**



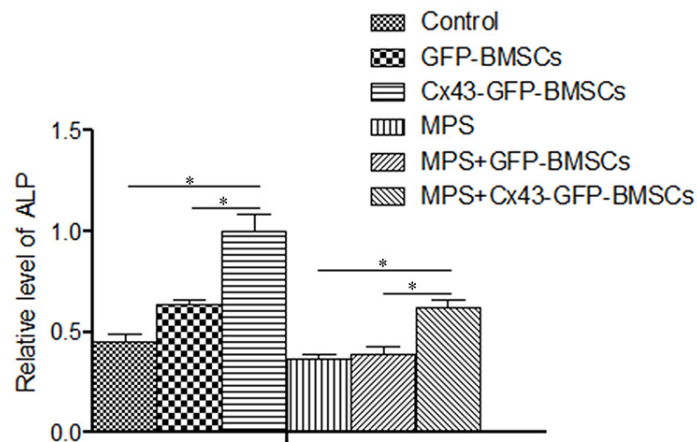
**C**



**D**



**E**



**F**

